Quantum Electronics **50** (10) 922–928 (2020)

INTERACTION OF LASER RADIATION WITH MATTER. LASER PLASMA https://doi.org/10.1070/QEL17344

Nonlinear Thomson scattering of a tightly focused relativistically intense laser pulse by an ensemble of particles

O.E. Vais, V.Yu. Bychenkov

Abstract. **We report a study of the process of nonlinear Thomson scattering (NTS) of a tightly focused relativistically intense laser pulse by an ensemble of electrons simulating the result of ionisation of an ultrathin nanofoil. The description of all six components of a laser pulse is based on the Stratton–Chu integrals describing radiation focused by an off-axis parabolic mirror into a spot down to the diffraction limit, which is of practical interest for modern experiments with extreme-intensity lasers, including diagnostics of their parameters. The interaction of a laser pulse with electrons is simulated by the test-particle method, and the resulting trajectories are used to calculate the characteristics of secondary electromagnetic radiation. The effect of the laser-pulse focal spot diameter in the range $\lambda-6\lambda$ on the angular distributions of the radiated energy and NTS spectra, as well as of a laser-beam peak intensity of 10^{21}–10^{22} W cm^{-2} on the spectral width of the secondary radiation is studied in relation to the experimentally implemented focusing scheme using the example of a laser pulse with an initial homogeneous spatial distribution and a duration of ~25 fs.**

Keywords: *tight focusing, relativistically intense laser pulse, direct acceleration of electrons, nonlinear Thomson scattering.*

1. Introduction

To date, the development of laser technologies has made it possible to exceed the petawatt power level of laser facilities [1]. The intensity of focused laser beams generated by such high-power systems has already reached $\sim 10^{22}$ W cm^{-2} [2–4] and is predicted to attain a level of 10^{23} W cm^{-2} in the years to come, which opens up a possibility of studying the interaction of laser pulses of extremely high energy density with matter. In some experimental configurations, effects that were insignificant at lower intensities come to the fore in the regime of interaction of particles with high-intensity radiation. They include the radiation friction force, which affects the dynamics of an electron [5], the production of electron–positron pairs, and other effects of quantum electrodynamics [6]. In addition, high-power laser systems of extreme intensity open up prospects for the development of new sources of high-energy particles (electrons, ions and neutrons) and secondary electromagnetic radiation in the processes of bremsstrahlung and betatron radiation, as well as of nonlinear Thomson scattering (NTS). This work is devoted to the study of the latter under conditions as close as possible to the conditions of the experiment.

The process of nonlinear Thomson scattering of a laser pulse on single electrons was studied in detail in the approximation of a plane electromagnetic wave [7, 8], in the paraxial approximation [9] including diffraction corrections taken into account [10], and using the exact solution of the Helmholtz equation to describe the components of the laser field [11]. The effect of the radiation friction force on the particle dynamics was also studied both in the co-propagating (when electrons move in the direction of laser pulse propagation or are at rest [12]) and counterpropagating (when electrons move towards the laser pulse [13]) geometries. It was shown that in the latter case this force has a significant effect on the generation of secondary radiation by electrons, leading to a decrease in its characteristic frequencies and power. The radiation generated in the NTS process has also been observed experimentally [14–16]. Until now, the laser radiation intensity in the performed experiments did not exceed 10^{20} W cm^{-2}, and the focal spot diameter remained sufficiently large (greater than 6λ), which made it possible to use approximate theoretical models to describe the laser pulse field at the focus and compare them with experimental results. To describe experiments with higher intensities and smaller focal spot diameters, it is undoubtedly necessary to develop an NTS theory that takes into account the effect of a strong spatial inhomogeneity of the laser beam near the focus on the particle dynamics.

One of the possible practical applications of the NTS effect is diagnostics of high-intensity laser pulses by measuring the angular-spectral characteristics of the secondary radiation generated during the interaction of a laser pulse with ultrathin nanofoils or a rarefied gas. Such an approach would make it possible to measure the laser beam characteristics 'directly', namely, without reducing its power or diverting part of the radiation into a separate channel, and would be an alternative, possibly with a number of advantages, to other 'direct' methods based, for example, on detecting multiple ionisation of particles [17–19] or measuring the angular-spectral characteristics of accelerated electrons or protons [20–25]. Based on the scheme of interaction of a laser pulse with counterpropagating electrons, Har-Shemesh and Di Piazza [26] showed theoretically and Yan et al. [27] confirmed experimentally the possibility of measuring the peak laser intensity by using the angular width of the NTS spectra. In addition, within the framework of the problem of diagnosing a laser pulse, Harvey [28] investigated the influence of polarisation, laser pulse duration, and electron energy on the angu-

O.E. Vais, V.Yu.Bychenkov Lebedev Physical Institute, Russian Academy of Sciences, Leninsky prosp. 53, 119991 Moscow, Russia; Center for Fundamental and Applied Research, Dukhov Automatics Research Institute (VNIIA), ul. Sushchevskaya 22, 127055 Moscow, Russia; e-mail: vajsoe@lebedev.ru

Received 25 March 2020; revision received 20 May 2020
Kvantovaya Elektronika **50** (10) 922–928 (2020)
Translated by I.A. Ulitkin

lar distribution of the secondary radiation energy. Krämer et al. [29] also proposed to use the NTS characteristics for diagnostics of the emittance of an electron beam, along with diagnostics of the laser radiation intensity. Nonlinear Thomson scattering by a chirped electron beam propagating perpendicular to the laser beam was proposed as a diagnostic method, but already of the laser pulse duration [30]. All of the above experimental configurations require preliminary acceleration of electrons and synchronisation of the laser pulse with the particle beam, in contrast to the scheme of interaction with practically resting electrons formed due to ionisation of a rarefied gas jet or ultrathin nanofoil. Such an interaction scheme of diagnosing the laser pulse intensity has already been implemented experimentally [31]. The laser beam was focused into a spot with a diameter of $\sim 30\lambda$, which made it possible to obtain theoretical estimates based on the approximation of a plane electromagnetic wave. The highest intensities of laser radiation are achieved in the case of its tight focusing that does not allow simple geometrical-optical or paraxial models to be used, which necessitates the study of the NTS effect of tightly focused laser radiation on an ensemble of particles, taking into account the exact description of the laser pulse components.

It is known from the linear theory of Thomson scattering that the spectrum of secondary radiation makes it possible to determine the energy distributions of electrons in a plasma due to the Doppler shift [32], which arises as a result of laser radiation scattering by moving particles. At the same time, when a high-intensity laser pulse interacts with particles at rest, electrons also gain energy, the value of which is determined by the intensity of laser radiation. Thus, the Doppler shift value in this case is related to the laser radiation intensity [33], which was experimentally demonstrated in the intensity range from 10^{18} to 10^{19} W cm^{-2} [31]. However, at relativistic intensities, nonlinear effects begin to make a significant contribution to the particle dynamics, leading to the formation of laser radiation harmonics in the NTS spectra. As the intensity increases, the maximum of the secondary radiation spectra shifts to the region of higher frequencies [8]. Consequently, the analysis and measurement of the characteristic NTS frequencies can form the basis of a new method for diagnosing the intensity of laser pulses, which is the subject of this work. The closest approach to the theory developed here is the simpler approach of Ref. [11], where the laser pulse was scattered by a single electron, which made it possible to qualitatively characterise the main NTS features. However, for the practical application of the proposed diagnostics, it is necessary to carry out a theoretical study of the scattering of a tightly focused laser beam by an ensemble of particles. The aim of this work is to analyse the spectral-angular distributions of the secondary radiation of an ensemble of electrons, as well as to examine the effect of the focal spot size of the laser pulse and its intensity on the NTS characteristics.

2. Model of nonlinear Thomson scattering by an ensemble of incoherent particles

We will describe the acceleration of electrons by a laser pulse within the framework of the test-particle method, neglecting the interaction forces between the particles, which turn out to be small compared to the laser field intensity when the light beam interacts with an ultrathin nanofilm or rarefied gas. In this case, the particle trajectories are calculated by solving the relativistic equation of motion with the Lorentz force:

$$\frac{\mathrm{d}m_\mathrm{e}\boldsymbol{v}\gamma}{\mathrm{d}t} = e\left(\boldsymbol{E} + \frac{[\boldsymbol{v}\times\boldsymbol{B}]}{c}\right),\ \frac{\mathrm{d}\boldsymbol{R}}{\mathrm{d}t} = \boldsymbol{v}, \tag{1}$$

where m_e and e are the mass and charge of the electron; $\boldsymbol{R}$, $\boldsymbol{v}$ and γ are the radius vector, velocity and gamma factor of the particle; c is the speed of light; and $\boldsymbol{E}$ and $\boldsymbol{B}$ are the electric and magnetic components of the laser pulse field. This model does not take into account the radiation friction force that can, if necessary, be included as an additional term in the right-hand side of the equation, which will be required at a laser radiation intensity of $I > 10^{23}$ W cm^{-2} [5]. The distributions of the field components of a focused laser beam are calculated using the Stratton–Chu diffraction integrals [34] in the form

$$\begin{aligned}\boldsymbol{E}(\boldsymbol{r},t) &= \int \boldsymbol{C}_\mathrm{e}(\boldsymbol{r},x',y')\boldsymbol{E}_i(x',y')\\ &\times\exp\{-\mathrm{i}[kl(\boldsymbol{r},x',y') - \omega_0 t + \phi_0]\}\,\mathrm{d}x'\mathrm{d}y',\\ \boldsymbol{B}(\boldsymbol{r},t) &= \int C_\mathrm{b}(\boldsymbol{r},x',y')\boldsymbol{B}_i(x',y')\\ &\times\exp\{-\mathrm{i}[kl(\boldsymbol{r},x',y') - \omega_0 t + \phi_0]\}\,\mathrm{d}x'\mathrm{d}y',\end{aligned} \tag{2}$$

where $\boldsymbol{E}_i(x',y')$ and $\boldsymbol{B}_i(x',y')$ are the amplitudes of the electric and magnetic components of the laser beam incident on the mirror; $l(\boldsymbol{r},x',y')$ is a function that describes the distance between a point on the mirror $[x',y',z'(x',y')]$ and an observation point (x,y,z); $\boldsymbol{C}_\mathrm{e}(\boldsymbol{r},x',y')$ and $\boldsymbol{C}_\mathrm{b}(\boldsymbol{r},x',y')$ are the tensors whose components depend on such mirror characteristics as the off-axis angle ψ_off and the effective focal length $F_\mathrm{eff} = 2F/(1+\cos\psi_\mathrm{off})$; F is the focal length of the 'parent' parabola; and ω_0 is the carrier frequency of the laser pulse. The integration limits correspond to the size of the incident beam. Detailed formulas for describing the laser pulse field are presented in Refs [22, 35], where the direct acceleration of electrons in the field of a laser pulse focused by an off-axis parabolic mirror is also discussed.

The acceleration of electrons is accompanied by the generation of secondary radiation in the process of Thomson scattering of a laser pulse on charged particles (Fig. 1). The power of radiation generated by a particle per unit solid angle can be calculated by the formula [36]

$$\frac{\mathrm{d}P(\boldsymbol{n},t')}{\mathrm{d}\Omega} \equiv \frac{cR_0^2|\boldsymbol{E}_\mathrm{r}|^2}{4\pi} = \frac{e^2}{4\pi c^3}\left|\left[\frac{\boldsymbol{n}\times[(\boldsymbol{n}-\boldsymbol{v}/c)\times\dot{\boldsymbol{v}}]}{(1-\boldsymbol{n}\boldsymbol{v}/c)^3}\right]_\mathrm{ret}\right|^2, \tag{3}$$

where $\boldsymbol{E}_\mathrm{r}$ is the electric component of the radiated field; $\dot{\boldsymbol{v}} = \mathrm{d}\boldsymbol{v}/\mathrm{d}t$ is the particle acceleration vector; $\boldsymbol{n}$ is a unit vector

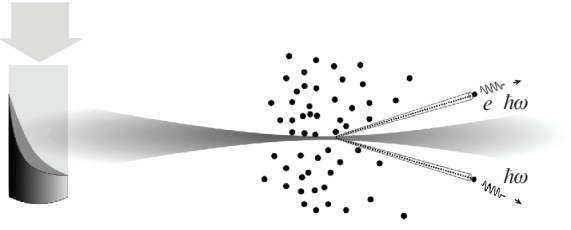

Figure 1. Schematic of NTS on an ensemble of electrons of a laser beam focused by an off-axis parabolic mirror.

in the observation direction; ret (from retarded) means that the expression in square brackets is taken at a retarded time $t' = t - (R_0 - \boldsymbol{nR})/c$; and R_0 is the distance between the emitting particle and the observation point. Integration of this characteristic over time gives the total energy emitted per unit solid angle:

$$\frac{\mathrm{d}W}{\mathrm{d}\Omega} = \int_{-\infty}^{\infty} \frac{\mathrm{d}P(\boldsymbol{n},t')}{\mathrm{d}\Omega}\mathrm{d}t'.$$

In the case of relativistic intensities, to which this work is devoted, the period of electron oscillations depends on the laser field strength [37]: $T \approx \lambda a_0^2/(4c)$ for $a_0 > 0$, where $a_0 = eE/(m_e c\omega_0)$. Therefore, under conditions of tight focusing, a strong spatial inhomogeneity of the laser pulse field leads to asynchronous oscillations of charged particles. Thus, the particles turn out to be incoherent with each other, which makes it possible to calculate the total energy of secondary radiation as an algebraic sum of N energies emitted by each individual particle:

$$\frac{\mathrm{d}W}{\mathrm{d}\Omega} = \sum_i^N \frac{\mathrm{d}W_i}{\mathrm{d}\Omega}.$$

The trajectories of electrons make it possible to carry out spectral analysis of secondary radiation by spectral decomposition of the emitted electric field:

$$\frac{\mathrm{d}^2 W(\boldsymbol{n},\omega)}{\mathrm{d}\Omega\mathrm{d}\omega} = \frac{cR_0^2\left|\int \boldsymbol{E}_\mathrm{r}\exp(\mathrm{i}\omega t)\,\mathrm{d}t\right|^2}{4\pi}$$

$$= \frac{e^2}{4\pi^2 c^3}\left|\int_{-\infty}^{\infty}\left[\frac{\boldsymbol{n}\times[(\boldsymbol{n}-\boldsymbol{v}/c)\times\dot{\boldsymbol{v}}]}{(1-\boldsymbol{nv}/c)^3}\right]_\mathrm{ret}\exp(\mathrm{i}\omega t)\,\mathrm{d}t\right|^2. \quad (4)$$

The spectrum of Thomson scattering by an ensemble of incoherent particles can also be obtained by summing the spectral amplitudes of the secondary radiation of individual electrons:

$$\frac{\mathrm{d}^2 W(\boldsymbol{n},\omega)}{\mathrm{d}\Omega\mathrm{d}\omega} = \sum_i^N \frac{\mathrm{d}^2 W_i(\boldsymbol{n},\omega)}{\mathrm{d}\Omega\mathrm{d}\omega}.$$

If the laser pulse intensity lies in the region of nonrelativistic values (i.e., if the dimensionless amplitude $a_0 < 1$, and the electron energy accumulated in such a field is much less than the particle rest energy), the nonlinear term in the Lorentz force (1) affects the particle dynamics insignificantly. In this case, the oscillation frequency of the particle turns out to be equal to the laser-pulse carrier frequency ω_0, and, as a consequence, the secondary radiation represents also electromagnetic waves with the frequency ω_0. However, with an increase in the laser radiation intensity up to the relativistic values, to which this work is devoted, the nonlinear term in the Lorentz force begins to play an essential role in the acceleration of the particle [37]. There is a transition to NTS, the spectrum of which is a set of harmonics [8], and the power is a set of ultrashort pulses of attosecond duration. Under conditions of tight focusing, the characteristics of the secondary radiation of an individual particle depend on both the laser radiation intensity and the size of its focal spot, which was shown in [11, 38]. The next section is devoted to the influence of these parameters on the characteristics of NTS of a laser pulse in an ensemble of particles.

3. Spectral-angular distributions of secondary radiation

Let us consider the Thomson scattering of a linearly polarised laser pulse with $\lambda = 0.8$ μm, a power of ∼200 TW, a pulse duration of ∼25 fs (at half the intensity), and a homogeneous initial spatial profile [$\boldsymbol{E}_i(x',y') = \mathrm{const}$], which was focused by an off-axis parabolic mirror (60° off-axis angle). The temporal envelope has the form

$$f(t,z) = \theta\left[1 - \frac{|k_0 z - \omega_0(t-\tau)|}{\omega_0\tau}\right]\cos^2\left[\frac{\pi}{2}\frac{k_0 z - \omega_0(t-\tau)}{\omega_0\tau}\right],$$

where τ is the laser pulse duration; $\theta(x)$ is the Heaviside function [22]; and $k_0 = \omega_0/c$. The laser pulse interacts with a monolayer of 10^4 electrons at rest. The monolayer is located perpendicular to the laser pulse propagation direction, and its transverse size is $10D_\mathrm{F} \times 10D_\mathrm{F}$, where D_F is the diameter of the focal laser spot at half the intensity. A similar model of interaction can be realised in an experiment using an ultrathin foil with a thickness $d \ll \lambda$ (where d is considerably smaller than the thickness of the relativistic skin layer $c\sqrt{a_0}\omega_\mathrm{p}$; and ω_p is the plasma frequency of the target electrons). In this case, we do not describe the ionisation of the foil by the laser field and neglect the energy loss due to ionisation, which is most acceptable for a material with a low ion charge (beryllium foil, diamond-like film, etc.).

We will describe the angular distributions of the secondary radiation in a spherical coordinate system (ϑ, φ) associated with the scattered laser pulse, where ϑ is the angle varying from 0 to 180° and measured from the laser pulse propagation direction, and φ is the angle in the plane perpendicular to this direction and measured from the direction of laser pulse polarisation.

One of the main features of NTS is the anisotropy of the radiated energy with respect to the angle φ, related to the laser radiation polarisation, which was demonstrated in [39] using the example of scattering of a plane electromagnetic wave. Figure 2 shows the angular distribution of the secondary radiation energy $\mathrm{d}W/\mathrm{d}\Omega$ generated as a result of scattering of 200 TW laser pulses having different sizes of the focal spot. As in the case of a plane wave, anisotropy is observed in the distribution of the secondary radiation energy, when, along the laser radiation polarisation direction ($\varphi = 0, \pi$), the scattered radiation is detected at larger angles ϑ than in the perpendicular direction.

The spectral NTS characteristics also depend on the observation direction, which is illustrated by the same example of the scattering of a laser pulse with a power of 200 TW. Figure 3 shows the spectra of the secondary radiation as functions of the observation angle ϑ along the direction of the laser pulse polarisation and perpendicular to it for $D_\mathrm{F} = 1.5\lambda$. The peak intensity in the considered case turns out to be equal to 10^{22} W cm^{-2}. Calculations showed that, under conditions of tight focusing at $\varphi = 0$, the spectra with the largest width are observed in two directions: at $\vartheta \sim 0$ and $\vartheta \lesssim \pi/6$. The latter direction will be determined by the angle ϑ_rad. Figure 4 shows the NTS spectra per particle. As follows from the calculations, although the radiation has a wider spectrum at the angle ϑ_rad, the secondary radiation propagating at small angles contains higher energy in the low-frequency region.

With an increase in the focal spot diameter, secondary radiation with a wide spectrum in the direction of small

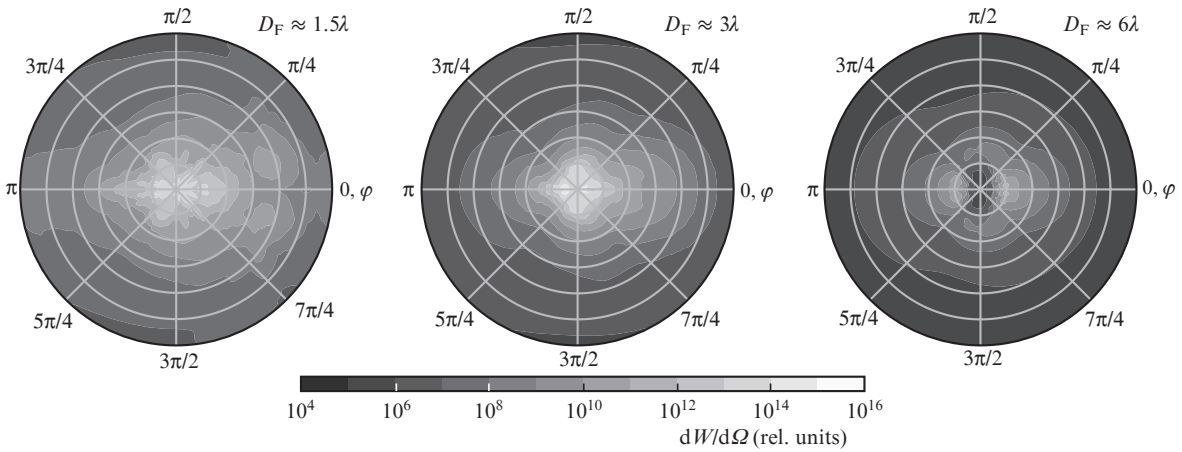

Figure 2. Angular distribution of the energy of secondary radiation of an electron ensemble upon scattering of a laser pulse with a duration of ~25 fs, a power of ~200 TW and different values of the focal spot diameter D_F. Concentric circles correspond to an angle ϑ ranging from 0 to 90°.

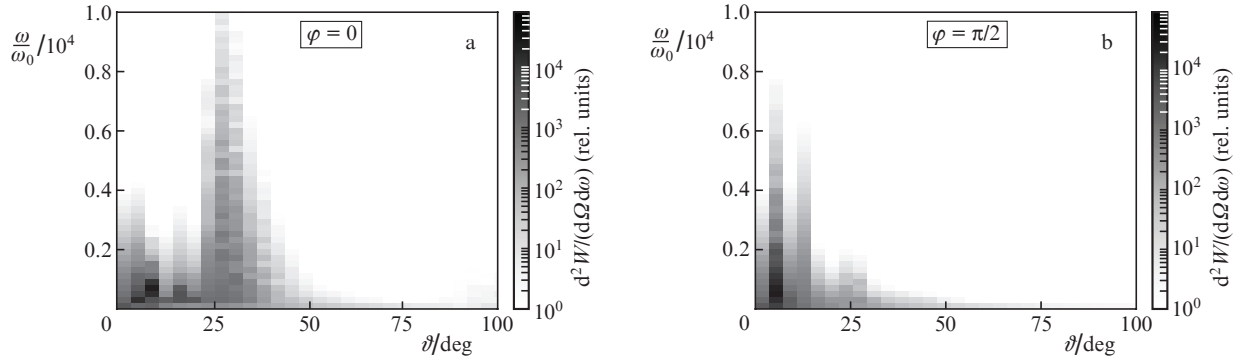

Figure 3. Spectra of secondary radiation, $d^2W/(d\Omega d\omega)$, generated during NTS on 10^4 particles, for different values of the observation angle ϑ (a) along the laser radiation polarisation direction (a) and (b) perpendicular to it. Laser pulse parameters are as follows: power, 200 TW; duration, 25 fs; peak intensity, 10^{22} W cm^{-2}; and $D_F = 1.5\lambda$.

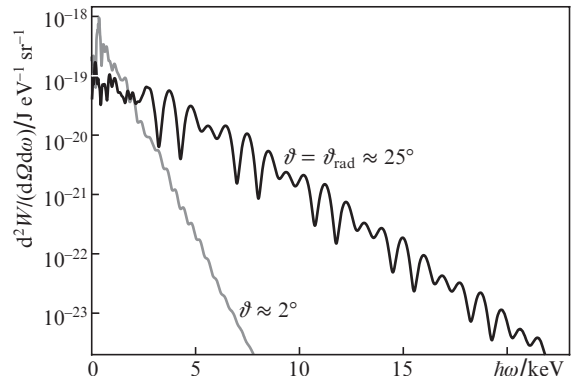

Figure 4. NTS spectra on an ensemble of particles per particle in the direction of polarisation of a laser pulse with a peak intensity of 10^{22} W cm^{-2}; $D_F = 1.5\lambda$.

angles is not generated, which follows from Fig. 5. The angle ϑ_{rad} changes as a function of the focal spot diameter: First, it decreases with an increase in D_F from λ to 4λ, and with further defocusing, it increases. A similar effect was observed for the direction of emission of high-energy particles directly accelerated by a laser pulse [22]. Table 1 shows the angle ϑ_{el} corresponding to the maximum of the angular distribution of accelerated electrons with energies exceeding 10 MeV, and the angle ϑ_{rad}. It follows from the table that these directions are close to each other, and the somewhat large numerical differences at small diameters of the focal spot can be explained by a wider angular distribution of fast electrons. Thus, it can be seen that the characteristics of radiation propagating at an angle ϑ_{rad} are determined by the dynamics of particles with the highest energy gain. Since the direction of emission of such particles depends on the laser spot diameter [22], the angle ϑ_{rad} also depends on it, which makes it possible to use this angle to estimate the laser spot diameter.

At $\varphi = \pi/2$, in the case of tight focusing ($D_F \approx 1.5\lambda$), the widest spectrum of secondary radiation is observed at small angles ϑ (see Fig. 3). With an increase in the focal spot diameter, a wide spectrum of secondary radiation in the direction perpendicular to the laser pulse polarisation is detected in a direction close to ϑ_{rad}; however, the spectral width turns out to be several times smaller than that observed along the laser pulse polarisation. In work [22], the φ-anisotropy of the distribution of fast particles with a maximum along the polarisation direction was demonstrated, which explains the larger spectral width of radiation along this direction than that in the direction $\varphi = \pi/2$.

For a given focal spot size, when the peak intensity of laser radiation changes, the φ-anisotropy of the energy and

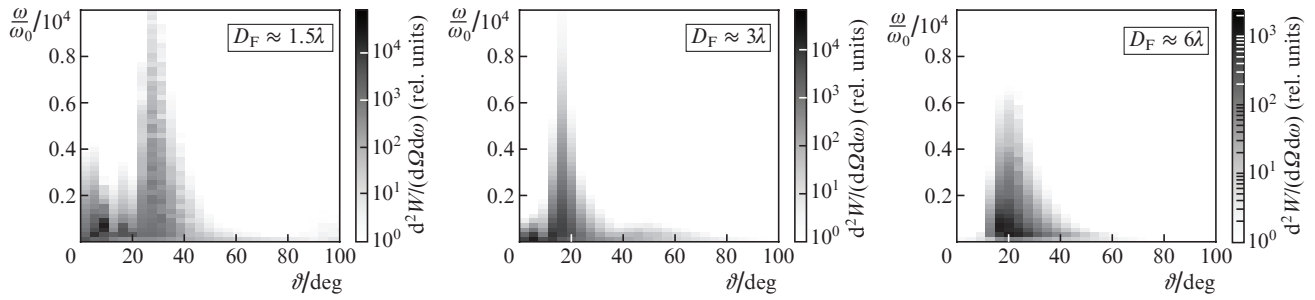

Figure 5. Spectra of secondary radiation, $d^2W/(d\Omega d\omega)$, generated during NTS on 10^4 particles, for different values of the observation angle ϑ along the laser radiation polarisation direction ($\varphi = 0$) at different D_F values of a laser pulse with a power of 200 TW and a duration of 25 fs.

Table 1. Emission angle ϑ_{el} of high-energy particles and angle ϑ_{rad}, at which the spectra of the secondary radiation in the laser pulse polarisation direction have the largest width, at different values of the focal spot diameter of the scattered laser pulse.

Angle/deg	D_F/λ					
	1.1	1.6	3.1	4.1	5.2	6.2
ϑ_{el}	27	19	12	10	13	17
ϑ_{rad}	36	25	15	11	16	16

spectra of secondary radiation is retained, which was confirmed by calculations. Figure 6, using $D_F \approx 1.5\lambda$ as an example, shows how a change in the intensity of laser radiation I_F affects the distribution of secondary radiation over the angle ϑ: A change in I_F from 10^{22} to 5×10^{21} W cm^{-2} is accompanied by a decrease in the width of the secondary radiation spectra while retaining the optimal viewing angles (small angle $\vartheta \approx 0°$ and angle $\vartheta_{rad} \approx 25°$); a further decrease in intensity leads to the fact that secondary radiation with the widest spectrum ceases to be generated in the ϑ_{rad} direction. The results obtained again indicate that the generation of secondary radiation in the ϑ_{rad} direction is associated with the dynamics of high-energy particles.

Corde et al. [39] showed that when use is made of the approximation of a plane electromagnetic wave, an increase in its intensity leads to a decrease in the width of the angular distribution of the secondary radiation energy (450 mrad for $a_0 = 5$ and 230 mrad for $a_0 = 10$) along the polarisation direction of the scattered laser radiation. However, when electrons interact with a tightly focused laser pulse, the electron drift direction does not coincide with the laser pulse propagation direction ($\vartheta = 0$), as in the case of a plane electromagnetic wave. The gradient of the laser pulse intensity leads to the repulsion of particles perpendicular to the light beam propagation direction [40], and therefore the accelerated electrons move along the surface of a cone whose axis coincides with the laser pulse propagation direction. As a result of such particle dynamics, the angular distribution of the radiated energy in the case of tight focusing has a maximum in a direction close to $\vartheta = 0$, for example, at $D_F \approx 1.5\lambda$, in contrast to the case of a longer focal system, for example, for $D_F \approx 6\lambda$, which is closer to the case of plane electromagnetic waves when the energy maxima are displaced relative to the laser pulse propagation direction along the polarisation vector. As the intensity increases, the appearance of high-energy particles moving and emitting at large angles leads to a broadening of the angular distribution of the secondary radiation energy, which is opposite to that observed in the case of scattering of a plane electromagnetic wave.

Let us consider how the brightness of the secondary radiation source depends on the laser radiation intensity. The results presented in this work were obtained under the assumption that the interaction of particles with a residual charge is negligible in comparison with their interaction with the laser pulse itself. If we were talking about interaction with a rarefied gas, then this would introduce a restriction on the concentration of particles in the volume:

$$n_e \ll n_{cr} \frac{a_0 \lambda}{D_F}, \tag{5}$$

where $n_{cr} = m_e \omega_0^2/(4\pi e^2)$ is the critical density of electrons (equal to 1.7×10^{21} cm^{-3} for $\lambda = 0.8$ μm); and n_e is the density of electrons.

In the case under study, we obtain a restriction on the nanofilm thickness:

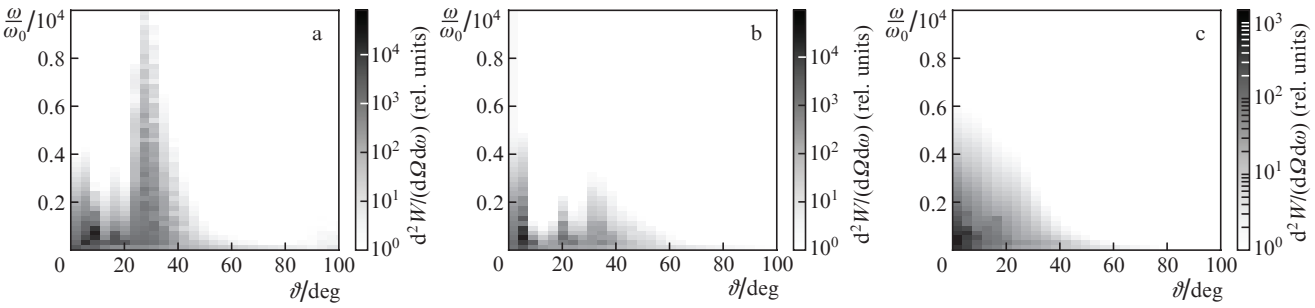

Figure 6. Spectra of secondary radiation $d^2W/(d\Omega d\omega)$ in the direction of laser polarisation ($\varphi = 0$) upon scattering of a 25-fs laser pulse with a focal spot diameter of 1.5λ at a peak laser intensity $I_F \approx$ (a) 10×10^{21}, (b) $\sim 5 \times 10^{21}$ and (c) $\sim 1 \times 10^{21}$ W cm^{-2}.

$$\Delta z \ll \Delta z_{\max} = \frac{a_0 n_{\rm cr}}{\pi n_{\rm e}}. \quad (6)$$

The introduced restrictions make it possible to estimate the number of emitting particles in a real target and, as a consequence, the brightness of the secondary radiation source. Figure 7 shows the brightness of the source of secondary radiation generated during NTS of a laser beam on an ultrathin nanofilm ($\Delta z \approx \Delta z_{\max}$, 1.34×10^{11} particles in a volume of $10D_{\rm F} \times 10D_{\rm F} \times \Delta z$) in the direction $(\varphi, \vartheta) = (0, \vartheta_{\rm rad})$ in a spectral interval equal to 0.1% of the emission spectrum width (0.1% BW) for various values of the peak intensity of laser radiation focused into a spot of 1.5λ in diameter ($\Delta z_{\max}$ was calculated for $I_{\rm F} = 10^{21}$ W cm^{-2}). It is seen that a decrease in the peak intensity leads to a decrease in the critical frequency, at which there is a sharp decrease in the intensity of the secondary radiation (on a double logarithmic scale). Thus, the considered critical frequency can be used to estimate the peak intensity of a laser pulse.

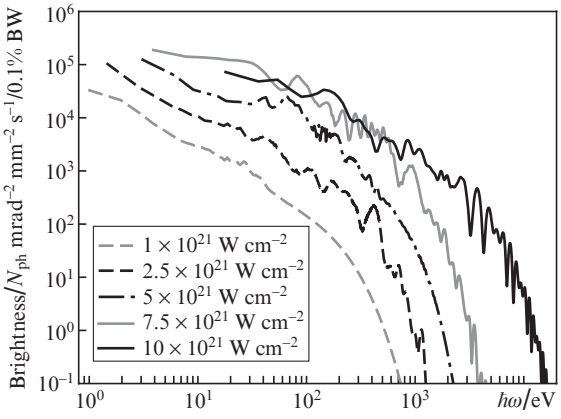

Figure 7. Brightness of the source of secondary radiation generated during NTS of a laser beam on an ultrathin nanofoil ($\Delta z \approx 0.1\Delta z_{\max}$, 1.34×10^{11} particles in a volume of $10D_{\rm F} \times 10D_{\rm F} \times \Delta z$) in the direction $(\varphi, \vartheta) = (0, \vartheta_{\rm rad})$ in the spectral interval equal to 0.1% of the emission spectrum width (0.1% BW) for different $I_{\rm F}$ values at a pulse duration of 25 fs and $D_{\rm F} = 1.5\lambda$.

The model used also did not take into account the effect of the radiation friction force, which imposes a limitation on the laser pulse intensity:

$$a_0 \ll \frac{3\lambda}{4\pi r_{\rm e}\gamma^2}, \quad (7)$$

where $r_{\rm e}$ is the classical radius of an electron. Condition (7) was obtained proceeding from the smallness of the radiation friction force $F_{\rm FF} \approx 2e^2\gamma^2\omega_2 a_0^2/(3c^2)$ [37] in comparison with the Lorentz force $F_{\rm L} \approx a_0 m_{\rm e}\omega c$. We showed in [22] that the considered parameters correspond to the condition of the model applicability. However, it should be noted that outside the framework (7) of the applicability of our consideration, the theoretical model, in principle, can be extended by taking into account the radiation friction force in the particle motion equation. This actually means that the limitation on the range of applicability of the proposed method for diagnosing laser pulses due to the force of radiation friction is removed.

In this work, we considered for definiteness a laser pulse with a temporal envelope proportional to the square of the cosine and a homogeneous initial spatial profile (since it is this profile that is quite often encountered in real experiments), which will make it possible to directly use the results obtained to quantitatively estimate the peak intensity and diameter of the focal spot in the case of laser pulses close to those considered here, as well as to qualitatively estimate the peak intensity for pulses without violations of the smoothness of the intensity envelope. However, it should be noted that Kharin et al. [41] showed in the framework of the plane electromagnetic wave approximation that, strictly speaking, the shape of the secondary radiation spectra depends on the temporal envelope of the laser pulse. Therefore, this method can potentially be used to diagnose the features of the temporal profile of a laser pulse, as well as its duration. Our proposed procedure for reconstructing the discussed pulse parameters makes this method universal and allows it to be used for various lasers. Note also that it was shown in [22, 35] that the energy distributions of electrons depend on the structure of the laser field near the focal spot. For example, low-intensity diffraction rings near the focus increase the number of particles with average energy. Therefore, we expect a similar response in the secondary radiation spectra, which can also be used to reveal possible features of the laser beam near the focal plane. Consequently, despite the fact that the calculations were carried out for a specific spatiotemporal shape of the laser pulse, the results obtained will be qualitatively correct for any slowly varying spatiotemporal shape, and for quantitative estimates necessary for diagnosing laser pulses, it will be necessary to carry out calculations taking into account the assumed shape of the laser pulse, which does not limit the proposed technique. Nevertheless, the issue of the influence of the spatiotemporal shape of a tightly focused laser pulse on the secondary radiation of electrons is undoubtedly important and rather extensive; therefore, it can serve as a topic for a separate publication.

4. Conclusions

We theoretically studied nonlinear Thomson scattering of a tightly focused laser pulse on an ensemble of charged particles in an ultrathin foil. A laser pulse with a homogeneous initial spatial profile was focused by an off-axis parabolic mirror. All six components of the laser field were calculated using the Stratton–Chu integrals, which allow one to describe the focusing of the laser beam down to the diffraction limit. In the calculations, the laser pulse interacted with a monolayer of free electrons, which can be realised in the experiment using a sufficiently thin target, where the field produced by the residual charge turns out to be small compared to the laser pulse field. In this case, the dynamics of particles and, consequently, the characteristics of the secondary radiation are determined by the parameters of the laser pulse, which makes it possible to further use the NTS characteristics for its diagnostics.

It was shown that, as in the case of scattering of a plane electromagnetic wave, the energy distribution of the secondary radiation under NTS of a tightly focused beam is anisotropic in the angle φ' and has a larger angular width along the polarisation direction of the laser pulse. At the same time, the size of the laser beam diameter affects the ϑ-distributions of the secondary radiation spectra, which have the largest width along the direction of propagation of high-energy particles.

Therefore, with a smaller diameter of the focal spot, secondary radiation with the largest spectral width should be detected at larger angles (at D_F in the range $\lambda - 4\lambda$). In the considered example with a peak laser power of 200 TW at $D_F > 5\lambda$, no further decrease in the angle ϑ_{rad} was observed. In addition, at small diameters of the focal spot, the secondary radiation also propagated along the direction of the laser pulse propagation, and with an increase in the diameter of the focal spot, the fraction of such radiation decreased. Therefore, detecting the propagation direction of the secondary radiation with a wide spectrum and the fraction of secondary radiation propagating forward will make it possible to estimate the diameter of the focal laser spot. The calculations showed an increase in the critical frequency of the secondary radiation in the ϑ_{rad} direction with an increase in the intensity of the scattered laser radiation, which can be used for its evaluation. Thus, an analysis of the angular distribution of secondary radiation and its spectral composition can form the basis of a new method for simultaneous diagnostics of the intensity of the laser pulse and the diameter of its focal spot.

Acknowledgements. This work was supported by the Russian Foundation for Basic Research (Grant Nos 18-32-00406 mol_a and 18-02-00452) and the Foundation for the Advancement of Theoretical Physics and Mathematics 'BASIS' (Grant No. 18-1-5-102-1).

References

1. Danson C.N., Haefner C., Bromage J., Butcher Th. *High Power Laser Sci. Eng*., **7**, e54 (2019).
2. Yanovsky V., Chvykov V., et al. *Opt. Express*, **16**, 2109 (2008).
3. Pirozhkov A.S., Fukuda Yu., et al. *Opt. Express*, **25**, 20486 (2017).
4. Yoon J.W., Jeon Ch., Shin J., et al. *Opt. Express*, **27**, 20412 (2019).
5. Di Piazza A., Hatsagortsyan K.Z., Keitel C.H. *Phys. Rev. Lett*., **102**, 254802 (2009).
6. Di Piazza A., Müller C., Hatsagortsyan K.Z., Keitel C.H. *Rev. Mod. Phys*., **84**, 1177 (2012).
7. Esarey E., Ride S.K., Sprangle P. *Phys. Rev. E*, **48**, 3003 (1993).
8. Lau Y.Y., He F., et al. *Phys. Plasmas*, **10**, 2155 (2003).
9. Galkin A.L., Korobkin V.V., Romanovskii M.Yu., Shiryaev O.B. *Quantum Electron*., **37**, 903 (2007) [*Kvantovaya Elektron*., **37**, 903 (2007)].
10. Harvey Ch., Marklund M., Holkundkar A.R. *Phys. Rev. Accel. Beams*, **19**, 094701 (2016).
11. Vais O.E., Bochkarev S.G., Bychenkov V.Yu. *Plasma Phys. Rep*., **42**, 818 (2016).
12. Golovinskii P.A., Mikhin E.A. *J. Exp. Theor. Phys*., **113**, 545 (2011) [*Zh. Eksp. Teor. Fiz*., **140**, 627 (2011)].
13. Koga J., Esirkepov T.Zh., Bulanov S.V. *Phys. Plasmas*, **12**, 093106 (2005).
14. Chen S., Maksimchuk A., Umstadter D. *Nature*, **396**, 653 (1998).
15. Ta Phuoc K., Rousse A., Pittman M., Rousseau J.P., Malka V., Fritzler S., Umstadter D., Hulin D. *Phys. Rev. Lett*., **91**, 195001 (2003).
16. Ta Phuoca K., Burgy F., Rousseau J.-P., Rousse A. *Eur. Phys. J. D*, **33**, 301 (2005).
17. Chowdhury E.A., Barty C.P.J., Walker B.C. *Phys. Rev. A*, **63**, 042712 (2001).
18. Yamakawa K., Akahane Y., Fukuda Y., Aoyama M., Inoue N., Ueda H. *Phys. Rev. A*, **68**, 065403 (2003).
19. Ciappina M.F., Popruzhenko S.V., Bulanov S.V., Ditmire T., Korn G., Weber S. *Phys. Rev. A*, **99**, 043405 (2019).
20. Galkin A.L., Kalashnikov M.P., Klinkov V.K., et al. *Phys. Plasmas*, **17**, 053105 (2010).
21. Kalashnikov M., Andreev A., et al. *Laser Part. Beams*, **33**, 361 (2015).
22. Vais O.E., Bychenkov V.Yu. *Appl. Phys. B*, **124**, 211 (2018).
23. Ivanov K.A., Tsymbalov I.N., Vais O.E., et al. *Plasma Phys. Control. Fusion,* **60**, 105011 (2018).
24. Mackenroth F., Holkundkar A.R., Schlenvoigt H.-P. *New J. Phys*., **21**, 123028 (2019).
25. Vais O.E., Thomas A.G.R., et al. *New J. Phys*., **22**, 023003 (2020).
26. Har-Shemesh O., Di Piazza A. *Opt. Lett*., **37**, 1352 (2012).
27. Yan W., Fruhling C., Golovin G., et al. *Nat. Photonics*, **11**, 514 (2017).
28. Harvey C.N. *Phys. Rev. Accel. Beams*, **21**, 114001 (2018).
29. Krämer J. M., Jochmann A., Budde M., et al. *Sci. Rep*., **8**, 1398 (2018).
30. Mackenroth F., Holkundkar A.R. *Sci. Rep*., **9**, 19607 (2019).
31. He C.Z., Longman A., et al. *Opt. Express*, **27**, 30020 (2019).
32. Glenzer S.H., Rozmus W., MacGowan B.J. *Phys. Rev. Lett*., **82**, 97 (1999).
33. Gao J. *Appl. Phys. Lett*., **88**, 091105 (2006).
34. Stratton J.A., Chu L.J. *Phys. Rev*., **56**, 99 (1939).
35. Vais O.E., Bochkarev S.G., Ter-Avetisyan S., Bychenkov V.Yu. *Quantum Electron*., **47**, 38 (2017) [*Kvantovaya Elektron*., **47**, 38 (2017)].
36. Jackson J.D. *Classical Electrodynamics* (New York: Wiley, 1962).
37. Landau L.D., Lifshitz E.M. *The Classical Theory of Fields* (Oxford: Pergamon Press, 1971).
38. Vais O.E., Bochkarev S.G., Bychenkov V.Yu. *Bull. Lebedev Phys. Inst*., **43**, 12 (2016) [*Kr. Soobshch. Fiz. FIAN*, (12), 52 (2015)].
39. Corde S., Ta Phuoc K., et al. *Rev. Mod. Phys*., **85**, 1 (2013).
40. Quesnel B., Mora P. *Phys. Rev. E*, **58**, 3719 (1998).
41. Kharin V.Yu., Seipt D., Rykovanov S.G. *Phys. Rev. A*, **93**, 063801 (2016).